Haline hurricane wake in the Amazon/Orinoco plume: AQUARIUS/SACD and SMOS observations

Semyon A. Grodsky[1], Nicolas Reul[2], Gary Lagerloef[3], Gilles Reverdin[4], James A. Carton[1], Bertrand Chapron[2], Yves Quilfen[2], Vladimir N. Kudryavtsev[5], and Hsun-Ying Kao[3]

[1]Department of Atmospheric and Oceanic Science, University of Maryland, College Park, USA
[2] Institut Francais pour la Recherche et l'Exploitation de la Mer, Plouzane, France
[3]Earth and Space Research, Seattle, Washington, USA
[4]Laboratoire d'Océanographie et de Climatologie par Expérimentation et Analyse Numérique, Institut Pierre Simon Laplace, CNRS/UPMC/IRD/MNHN, Paris, France.
[5]Russian State Hydrometeorological University and Nansen International Environmental & Remote Sensing Centre, St Petersburg, Russia
Corresponding author: senya@atmos.umd.edu

Abstract

At its seasonal peak the Amazon/Orinoco plume covers a region of 10^6 km^2 in the western tropical Atlantic with more than 1m of extra freshwater, creating a near-surface barrier layer (BL) that inhibits mixing and warms the sea surface temperature (SST) to >29^{o}C. Here new sea surface salinity (SSS) observations from the Aquarius/SACD and SMOS satellites help elucidate the ocean response to hurricane Katia, which crossed the plume in early fall, 2011. Its passage left a 1.5psu high haline wake covering >10^5 km^2 (in its impact on density, the equivalent of a 3.5^{o}C cooling) due to mixing of the shallow BL. Destruction of this BL apparently decreased SST cooling in the plume, and thus preserved higher SST and evaporation than outside. Combined with SST, the new satellite SSS data provide a new and better tool to monitor the plume extent and quantify tropical cyclone upper ocean responses with important implications for forecasting.

1. Introduction

Because of the importance of latent heat release as an energy source, hurricane strength depends on changes in the underlying ocean thermal stratification (e.g. Shay et al., 2000,

Saunders and Lea, 2008). Intense hurricane-induced mixing and upwelling act to entrain cool thermocline water into the mixed layer, leaving behind a cool wake of SST depressed by a few degrees, which reduces hurricane growth potential (e.g. Price, 1981; Bender and Ginis, 2000; Zhu and Zhang, 2006). Passage over freshwater plumes generally causes strengthening of hurricanes due to high SST (Ffield, 2007; Vizy and Cook, 2010) and minimization of the cool wake due to the presence of the BL (Sengupta et al., 2008; Wang et al., 2011; Balaguru et al., 2012). These produce nearly 50% increase in intensification rate over BL regions and occur in 10-20% of tropical cyclone cases worldwide (Balaguru et al., 2012), but are more probable (68%) for the most intense (category 5) hurricanes (Ffield, 2007). Here we combine newly available SSS from the Aquarius/SACD and SMOS missions together with other in situ and remote sensing observations to explore the impact of the Amazon/Orinoco plume on spatial and temporal signatures of SSS and SST after the passage of hurricane Katia in fall, 2011. We expect that new ability to map the plume more precisely with satellite SSS will benefit hurricane forecasting when it is evident that the trajectory will intersect the plume at some stage.

Unlike SST widely available from remote sensing, SSS is relatively sparse and its response to passing storms is often overlooked. Recognition of the impact of hurricane on a BL goes back at least to sample profile observations of Price (1981) showing the breakdown of a BL in the Gulf of Mexico. A similar Argo record was presented by McPhaden et al. (2009) in the Bay of Bengal. But, compared to ARGO or moorings, the satellite SSS now enables tracking the spatial variability of SSS induced by hurricanes in an unprecedented manner.

The western tropical Atlantic is characterized by high SST>29^{o}C, and a plume of low SSS caused by Amazon and to a lesser extent Orinoco river discharge as well as local rainfall (Yoo and Carton, 1990; Dessier and Donguy, 1994; Lentz, 1995; Foltz and McPhaden, 2008). This freshwater forcing produces a strong halocline in the upper 3-30m, below which salinity

exceeds 36psu. The plume deepens seaward and acts as a BL in density whose presence is associated with elevated SST (Pailler et al., 1999; Mignot et al., 2012). The plume extends eastward from the mouth of the Amazon at 0-2^{o}N, 50^{o}W with widths of 200-300km in June through December when Amazon discharge is at a seasonal minimum (0.08×10^6 m^3/s in November), expanding to 400-500km in March to May when Amazon discharge reaches a seasonal maximum of 0.24×10^6 m^3/s and winds are weak (Hu et al., 2004; Salisbury et al., 2011). At this rate of discharge an area of 10^6 km^2 is diluted by 2psu down to the 20m depth in around two months. Further north the seasonality of the plume is the reverse in that it reaches its maximum northward and eastward extent from the coast in August-September when the zone of weak winds shifts northward. The plume contracts in November, which is coincident with the reappearance of the northeast trade winds and shifts in the surface currents (Dessier and Donguy, 1994).

The hurricane season in the Atlantic extends from early June through the end of November, with a peak in late August - early September. The most intense hurricanes, according to the National Hurricane Center (NHC), form off the Cape Verde Islands in the eastern basin in fall, growing as they progress westward across the warm SSTs. In 2011, the first of two Cape Verde hurricanes and the second hurricane of the season began as tropical storm, Katia, in late August. Katia reached a Category 1 on September 1 with minimum central pressure of $P_{\min}$=988mb and the radius of sustained hurricane force winds R=55km. By the afternoon of September 4, Katia reached a Category 2 (maximum sustained winds > 44m/s, $P_{\min}$=961mb, and R=75km). By the evening of September 5, after passing over the freshwater plume, Katia had strengthened to a Category 4 (winds >60m/s, $P_{\min}$=942mb, and R=95km). Twenty-four hours later, Katia weakened to a Category 1. Here we examine the response of the upper ocean to the passage of Katia as it appears in the in situ and satellite records.

2. Data

SSS is provided by US/Argentina Aquarius/SACD (Lagerloef et al., 2008; Lagerloef 2012, Lagerloef et al., 2012) and the ESA Soil Moisture and Ocean Salinity (SMOS, Reul et al., 2012a) missions. Aquarius daily L3 SSS (ftp://saltmarsh.jpl.nasa.gov/L3/mapped/V1.3) is available since 25 August, 2011 and provides global coverage every week on a 1^o x 1^o grid. Higher resolution 0.2^o x 0.2^o bias corrected SSS (Lagerloef, 2012; Lee et al., 2012) is compiled for two weeks encompassing the passage of Katia. SMOS was launched in November, 2009. It has average resolution of 43 km and provides global coverage every 3 days. Here we use L3 SMOS SSS from 'Centre Aval de Traitement des Données SMOS' (CATDS, www.catds.fr, see documentation at www.salinityremotesensing.ifremer.fr/documentation-cec-products).

Both sensors operate in the 21 cm microwave L-band and thus sample salinity in the upper few centimeters of the ocean. Since surface roughness strongly affects L-band brightness temperature (Lagerloef et al., 2008; Reul et al., 2012a), and SMOS does not measure it, SSS is estimated with a 1 to 2 days lag after hurricane passage to allow the sea state to calm. Despite this roughness-dependence, L-band frequencies have a compensating advantage in that they are less affected by clouds and rain than higher frequencies, and thus can be used to infer stormy winds (Reul et al., 2012b).

The accuracy of the 10-day SMOS SSS is ~ 0.3 psu in the tropics (Reul et al., 2012a). The accuracy of Aquarius SSS is assessed in the Supplements by comparison to in situ ~1m depth salinity from the Indian, Atlantic, and Pacific tropical moorings, during August, 2011 - May, 2012. RMS difference of weekly Aquarius SSS is < 0.25psu, with a slight 0.1psu negative bias relative to in situ salinity. The bias is stronger in regions of low SSS, as expected, where intense rainfall produces the freshwater lenses (Henocq et al., 2010; Reverdin et al., 2012). Comparison of the much more limited set of 121 spatially and temporally collocated Argo and

Aquarius during September to November, 2011 suggests a somewhat larger range of differences. Prior to its use in this study the temporal variations of Aquarius SSS averaged zonally and with latitude in the band 50°S-50°N are removed to lessen the impact of a known 0.2psu time-dependent bias (due to an unaccounted for component of radiometer drift, D. Levine, Personal Communication, 2012). To increase stability and accuracy we only use weekly average Aquarius SSS.

Fig. 1 illustrates a comparison of the two satellite SSSs with in situ 5m depth thermosalinograph (TSG) along a ship track passing through 500km of the Amazon plume (8°-13°N) during which the intake salinity drops by 3-4psu to well below 34psu. The coincident satellite SSSs show a similar signature of the plume, although displaced slightly southward (however this apparent shift may result from the SSS spatial and temporal averaging).

In addition to SSS we examine daily SST based on satellite microwave and infrared and in-situ data, available at 0.25°x0.25° resolution (Reynolds et al., 2007) and TRMM Microwave Imager (TMI) SST (www.ssmi.com/tmi/tmi_browse.html). Daily 0.25°x0.25° L3 Advanced SCATterometer (ASCAT) 10m neutral winds of Bentamy and Croize-Fillon (2012) are available at ftp.ifremer.fr/ifremer/cersat/products/gridded/MWF. In-situ vertical profiles of temperature and salinity are provided by the Argo Program (Roemmich et al., 2009).

3. Results

During our records (**Fig. 2a**), the region of low SSS< 34psu in the plume has a maximum area >10^6 km^2 extending northward to 20°N and westward into the Caribbean (partly due to the contribution of the Orinoco), and is mainly confined to regions where SST>29°C (**Fig. 2b**). The plume extends eastward to 40°W along the North Equatorial Countercurrent in the latitude band 5°-10°N. It is separated from the coast by a few hundred kilometer wide patch of higher salinity evident along the transect in **Fig. 1**. This plume differs from the September climatology of

Dessier and Donguy (1994) by the generally lower SSS (confirmed by in-situ data in **Fig. 1**) and the further northward extension in the 1000 km wide longitude band between 60^{o}-50^{o}W. The plume area exceeds 10^{6} km^{2} when the wind speed has a monthly minimum of 3m/s in September, 2011 (**Fig. 2c**). After September the winds strengthen as the northeasterly trades reappear and, consistent with the Dessier and Donguy (1994) climatology, the area of the plume decreases perceptibly (in part due to stronger wind mixing), reaching a minimum in January-March, 2012 (**Fig. 2c**).

As tropical storm Katia approached the plume from the east (August 30 - September 2, **Figs. 3a,d**) its cool wake was relatively weak $< 0.5^{o}$C (comparing the week prior to the week following **Figs. 3c,f**). The oceanic response changed on September 2 as the storm entered the region of the plume and rapidly strengthened to Category 2. SST under the hurricane initially increased to 28.5^{o}C, while the cooling intensified to ~1^{o}C (**Figs. 3c,f**). Hurricane-induced mixing caused a 1-2psu rise in SSS in the plume (**Figs. 3b,e**) and Katia continued to strengthen to Category 4 by September 4. SST cooling rapidly amplified to ~2^{o}C as the hurricane left the plume area (**Figs. 3c,f**).

The strong SSS increase in hurricane wake within the plume (**Figs. 3, 4**) is explained by an erosion of the BL. This is evident by Argo profiles collected within the plume (**Fig. 5**, #1, #3, see also Supplementary Material Fig. S3 for location #2) that indicate the presence of shallow, about 15m deep mixed layer overlying the halocline. Mixed layer salinity is lower by 2 to 4 psu than the water beneath. This shallow haline stratification is destroyed by hurricane-forced entrainment (mixed layer deepening and upwelling), which is stronger on the right side of hurricane eye. Although the hurricane strengthened further along the trajectory, the SSS change is much weaker there corresponding to weak vertical salinity stratification outside the plume (**Fig. 5**, #8 and supplemental Fig.S3, #7).

On the left side of the trajectory there is an area of SSS decrease (**Fig. 4**) sampled by Argo #4 and #5. In contrast to the increase in SSS within the plume where the BL is eroded, the surface (down to 30m, **Fig. 5** #5) adjacent to the northwestern corner of the plume is 1psu fresher after the passage of hurricane. The decrease in salinity implies an addition of 1m of freshwater, much larger than could have come from direct rainfall. The most likely explanation is freshwater advection from the plume with some additional contribution due to direct rainfall.

Magnitude of SSS increase in the haline wake (about 1.5 psu, **Fig. 4**) agrees with the vertical salinity change of 3 to 4 psu (found in the vertical profiles within the plume, **Fig. 5** #1 and #3) for mixing penetrating down to twice the initial halocline depth. SSS changes observed by Aquarius and SMOS qualitatively well agree (**Fig. 4**) suggesting that satellite sensing of SSS is a mature technique for strong signals >1 psu.

The thermal wake is detectable along the entire hurricane track and gradually intensifies with the intensifying hurricane, but the haline wake is mostly confined to the plume (**Fig. 6**). In the week following hurricane passage the SST cooling is less pronounced in the plume where SST remains warmer by 0.5^{o}C than SST outside (**Fig. 6b**). The shallower vertical stratification of salinity acts to reduce SST cooling (because extra work required to mix the BL), and thus impacts hurricane growth by weaker negative feedback, an interpretation consistent with Sengupta et al. (2008), Wang et al. (2011), and Balaguru et al. (2012).

4. Summary/Conclusions

About 68% of hurricanes that finally reached category 5 have crossed the Amazon/Orinoco plume (Ffield, 2007) where the presence of BL can enhance their growth rate by 50% (Balaguru et al., 2012), Here we present a case study of the passage of hurricane Katia over the plume for which an extensive array of remote sensed and in situ observations are available, in particular new SSS from SMOS and Aquarius. A similarly strong haline wake event was detected with

SMOS alone following hurricane Igor in September, 2010 (www.esa.int/esaEO/SEMJFHWX7YG_index_1.html#subhead3). The availability of SSS from both, SMOS and Aquarius reinforces these first observations and demonstrates spatial and temporal patterns of hurricane-BL interactions in an unprecedented manner. We find that both Igor and Katia forced SSS changes > 1 psu over an area exceeding 10^5 km^2. These abrupt changes last and have implications for SSS climate, since SSS is not damped like SST.

These observations confirm that over the plume a uniform density mixed layer is shallower than uniform temperature layer because of stable halocline, acting to inhibit cooling and vertical mixing. Under an intense hurricane the halocline, which is above the thermocline, is mixed first. This produces a SSS wake that is by a few psu saltier than initial SSS in the plume. From space-time diagrams of SSS and SST along the hurricane track we find that haline wake develops only within the plume and is associated with at least 0.5^{o}C weaker SST cooling than outside the plume. This difference in SST cooling is explained by additional work required to mix the BL. Thus BL leads to a reduction in hurricane-induced surface cooling that favors hurricane development, as the resulting elevated SST and high evaporation enhance the hurricane's maximum potential intensity.

The geographic location and seasonality of the Amazon/Orinoco plume makes hurricane overpasses a not-infrequent occurrence. Indeed, the expansion of the plume in August-September coincides with the peak of the production of Cape Verde hurricanes, a group which includes many of the most intense (Category 4-5) hurricanes. Thus the results presented here strongly suggest that the salinity stratification role in mixed layer dynamics should be taken into account when forecasting hurricane growth over the plume. The availability of satellite SSS from Aquarius and SMOS along with in situ ARGO measurements is critical to making such model improvements practical.

Acknowledgements This research was supported by NASA (NNX12AF68G, NNX09AF34G), ESA/ESRIN (AO/1-6704/11/I-AM), CNES support to CATDS, and Russian Government (11.G34.31.0078). TSG data are provided by ESA's SMOS Cal/Val effort supported by the CNES/TOSCA program and are collected from merchant vessels by the SSS observatory supported by IRD and INSU. TSG data were prepared by Denis Diverrès and Gaël Alory. We thank Da-Lin Zhang for comments on an earlier version of this manuscript.

References

Balaguru, K., P. Chang, R. Saravanan, L. R. Leung,, Z. Xu, M. Li, and J.-S. Hsieh, 2012: Ocean barrier layers' effect on tropical cyclone intensification, *PNAS*, 10.1073/pnas.1201364109.

Bender, M. A., and I. Ginis, 2000: Real-Case Simulations of Hurricane–Ocean Interaction Using A High-Resolution Coupled Model: Effects on Hurricane Intensity. *Mon. Wea. Rev.*, **128**, 917–946.

Bentamy, A., and D. Croize-Fillon, 2012: Gridded surface wind fields from Metop/ASCAT measurements. *Int. J. Remote Sens*., **33**, 1729-1754.

Dessier, A., and J.R. Donguy, 1994: The sea surface salinity in the tropical Atlantic between 10S and 30N – seasonal and interannual variations (1977 – 1989), *Deep Sea Res. I*, **41**, 81 – 100.

Ffield, A., 2007: Amazon and Orinoco River plumes and NBC Rings: bystanders or participants in hurricane events? *J. Clim*., **20**, 316-333.

Foltz, G. R., and M. J. McPhaden, 2008: Seasonal mixed layer salinity balance of the tropical North Atlantic Ocean, *J. Geoph. Res.*, **113**, C02013.

Henocq, C., J. Boutin, G. Reverdin, F. Petitcolin, S. Arnault, and P. Lattes, 2010: Vertical variability of near-surface salinity in the tropics: Consequences for L-band radiometer calibration and validation, *J. Atmos. Ocean. Techn.,* **27**, 192–209.

Hu, C., E. T. Montgomery, R. W. Schmitt, and F. E. Muller-Karger (2004), The dispersal of the Amazon and Orinoco River water in the tropical Atlantic and Caribbean Sea: Observation from space and S-PALACE floats, *Deep Sea Res. II*, **51**, 1151-1171.

Lagerloef, G., and Coauthors, 2008: The Aquarius/SAC-D Mission: Designed to meet the salinity remote-sensing challenge. *Oceanogr.*, **21**, 68–81.

Lagerloef, G., 2012:, Satellite Mission Monitors Ocean Surface Salinity, *EOS Trans. AGU,* **93** (25), 233-234.

Lagerloef, G., F. Wentz, S. Yueh, H.-Y. Kao, G. C. Johnson, and J. M. Lyman, 2012: Aquarius satellite mission provides new, detailed view of sea surface salinity, in State of the Climate 2011, *Bull. Amer. Meteor. Soc*., **93** (7), S70-S71.

Lee, T., G. Lagerloef, M. M. Gierach, H.-Y. Kao, S. Yueh, and K. Dohan (2012), Aquarius reveals salinity structure of tropical instability waves, *Geoph. Res. Lett*., **39**, L12610.

Lentz, S.J., 1995: Seasonal variations in the horizontal structure of the Amazon plume inferred from historical hydrographic data, *J. Geoph. Res*., **100**, 2391-2400.

Lumpkin, R., and Z. Garraffo, 2005: Evaluating the Decomposition of Tropical Atlantic Drifter Observations. *J. Atmos. Ocean. Techn.*, **22**, 1403–1415.

McPhaden, M. J., G. R. Foltz, T. Lee, V. S. N. Murty, M. Ravichandran, G. A. Vecchi, J. Vialard, J. D. Wiggert, and L. Yu, 2009: Ocean-Atmosphere Interactions During Cyclone Nargis, *Eos Trans. AGU*, **90**(7), 53.

Mignot, J., A. Lazar, and M. Lacarra, 2012: On the formation of barrier layers and associated vertical temperature inversions: A focus on the northwestern tropical Atlantic, *J. Geoph. Res.,* **117**, C02010.

Pailler, K., B. Bourlès, and Y. Gouriou, 1999: The barrier layer in the western tropical Atlantic Ocean, *Geoph. Res. Lett.*, **26**, 2069–2072.

Price, J. F., 1981: Upper ocean response to a hurricane, *J. Phys. Oceanogr.,* **11**, 153-175.

Reul, N., J. Tenerelli, J. Boutin,; B. Chapron, F. Paul, E. Brion, F. Gaillard, and O. Archer, 2012a: Overview of the first SMOS sea surface salinity products. Part I: quality assessment for the second half of 2010, *IEEE Trans. Geosci. Rem. Sens.*, **50**, 1636-1647.

Reul, N., J. Tenerelli, B. Chapron, D. Vandemark, Y. Quilfen, and Y. Kerr (2012b), SMOS satellite L-band radiometer: A new capability for ocean surface remote sensing in hurricanes, *J. Geoph. Res*., **117**, C02006.

Reverdin, G., S. Morisset, J. Boutin, and N. Martin, 2012: Rain-induced variability of near sea-surface T and S from drifter data, *J. Geoph. Res.,* **117**, C02032.

Reynolds, R.W., T.M. Smith, C. Liu, D. B. Chelton, K. S. Casey, and M. G. Schlax., 2007: Daily high-resolution-blended analyses for sea surface temperature, *J. Clim.*, **20**, 5473-5496.

Roemmich, D., and the Argo Steering Team, 2009: Argo: The challenge of continuing 10 years of progress, *Oceanography*, **22**, 46–55.

Salisbury, J., D. Vandemark, J. Campbell, C. W. Hunt, D. Wisser, N. Reul, and B. Chapron. 2011: Spatial and temporal coherence between Amazon River discharge, salinity, and light absorption by colored organic carbon in western tropical Atlantic surface waters. *J. Geoph. Res.*, **116**, C00H02.

Saunders, M.A., and A.S. Lea, 2008: Large contribution of sea surface warming to recent increase in Atlantic hurricane activity, *Nature*, **451**, 557-560.

Sengupta, D, B.R. Goddalehundi, D.S. Anitha (2008) Cyclone-induced mixing does not cool SST in the post-monsoon north Bay of Bengal, *Atmos. Sci. Letts.,* **9**, 1–6.

Shay, L.K., G.J. Goni, and P.G. Black, 2000: Effects of a warm oceanic feature on hurricane Opal, *Mon. Wea. Rev*., **128**, 1366-1383.

Vizy, E. K., and K. H. Cook (2010), Influence of the Amazon/Orinoco Plume on the summertime Atlantic climate, *J. Geoph. Res.*, **115**, D21112.

Wang, X-D., G. Han, Y.-Q. Qi, and W. Li, 2011: Impact of barrier layer on typhoon-induced sea surface cooling, *Dyn. Atmos. Ocean*, **52**, 367-385.

Yoo, J.-M., and J.A. Carton, 1990: Annual and interannual variation of the freshwater budget in the tropical Atlantic and Caribbean Sea, *J. Phys. Oceanogr.*, **20**, 831-845.

Zhu, T, and D.-L. Zhang, 2006: The impact of the storm-induced SST cooling on hurricane intensity, *Adv. Atmos. Sci.,* **23**, 14-22.

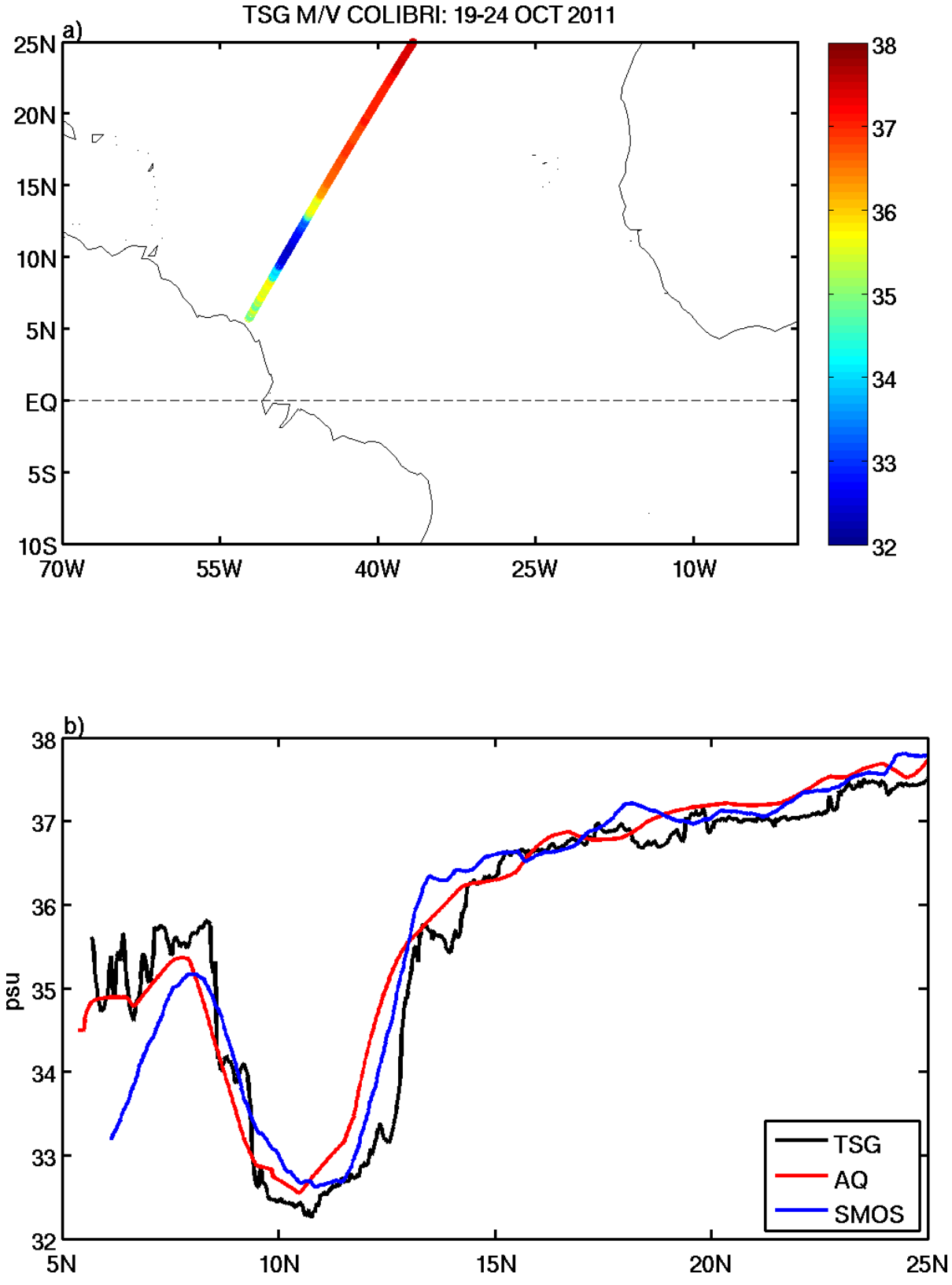

Figure 1. (a) Thermosalinograph (TSG) transect along Europe-French Guiana shipping route collected by vessel COLIBRI. Color indicates value of salinity. (b) TSG data with collocated weekly running mean AQUARIUS (AQ) and SMOS SSS.

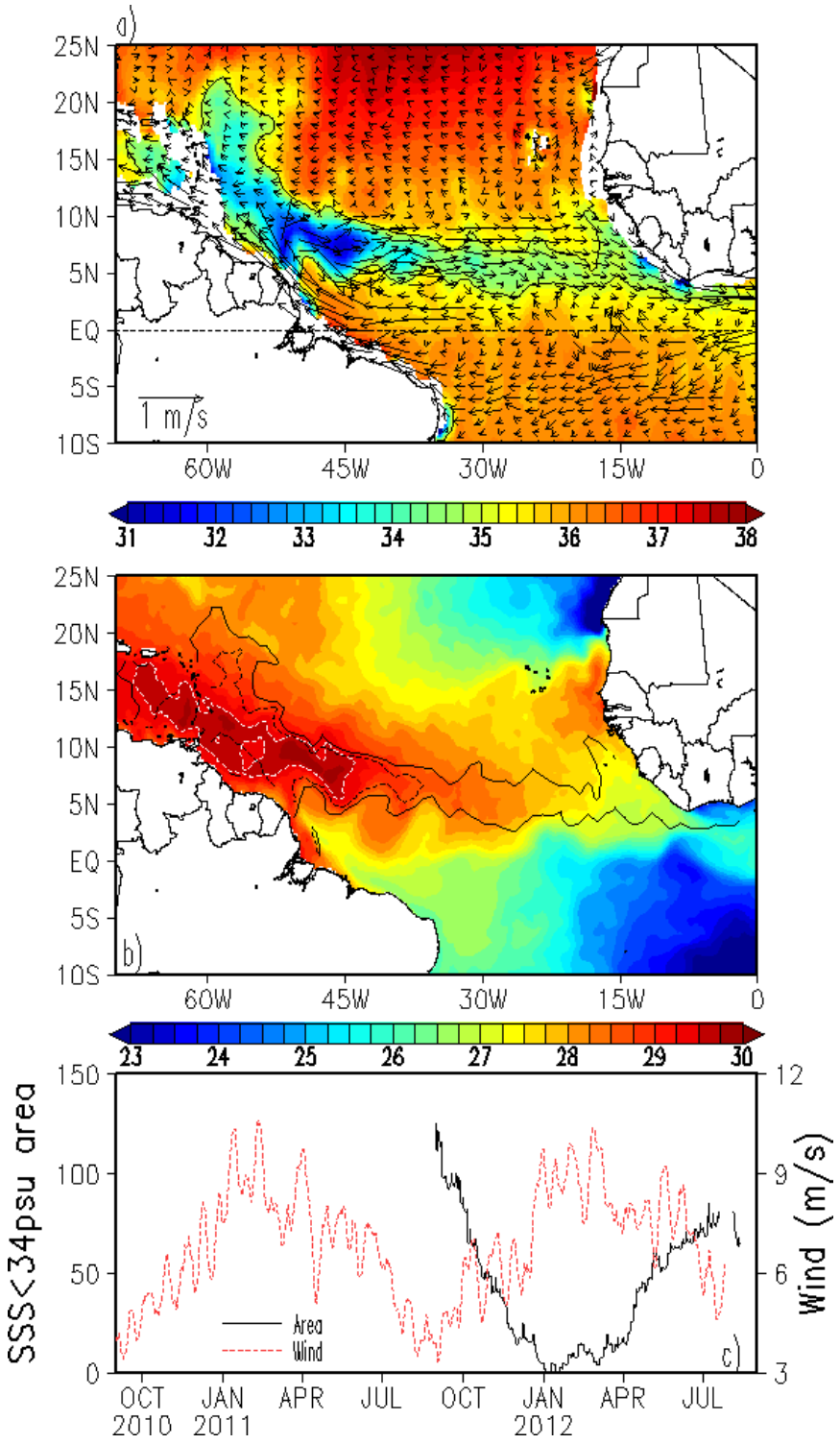

Figure 2. September 2011 mean (a) AQUARIUS SSS (shaded, psu) with September surface currents of Lumpkin and Garraffo (2005) overlain; (b) SST (shaded, degC), 34 psu (dashed, black) and 35psu (solid, black) contours are overlain, 'hot spots' SST>29.5C are emphasized. (c) Fresh water area (number of 1^{o}x1^{o} deg^{2} boxes within 34psu contour) and winds averaged over the September 2011 SSS<34psu area (shown in panel b). Land-contaminated coastal data are blanked.

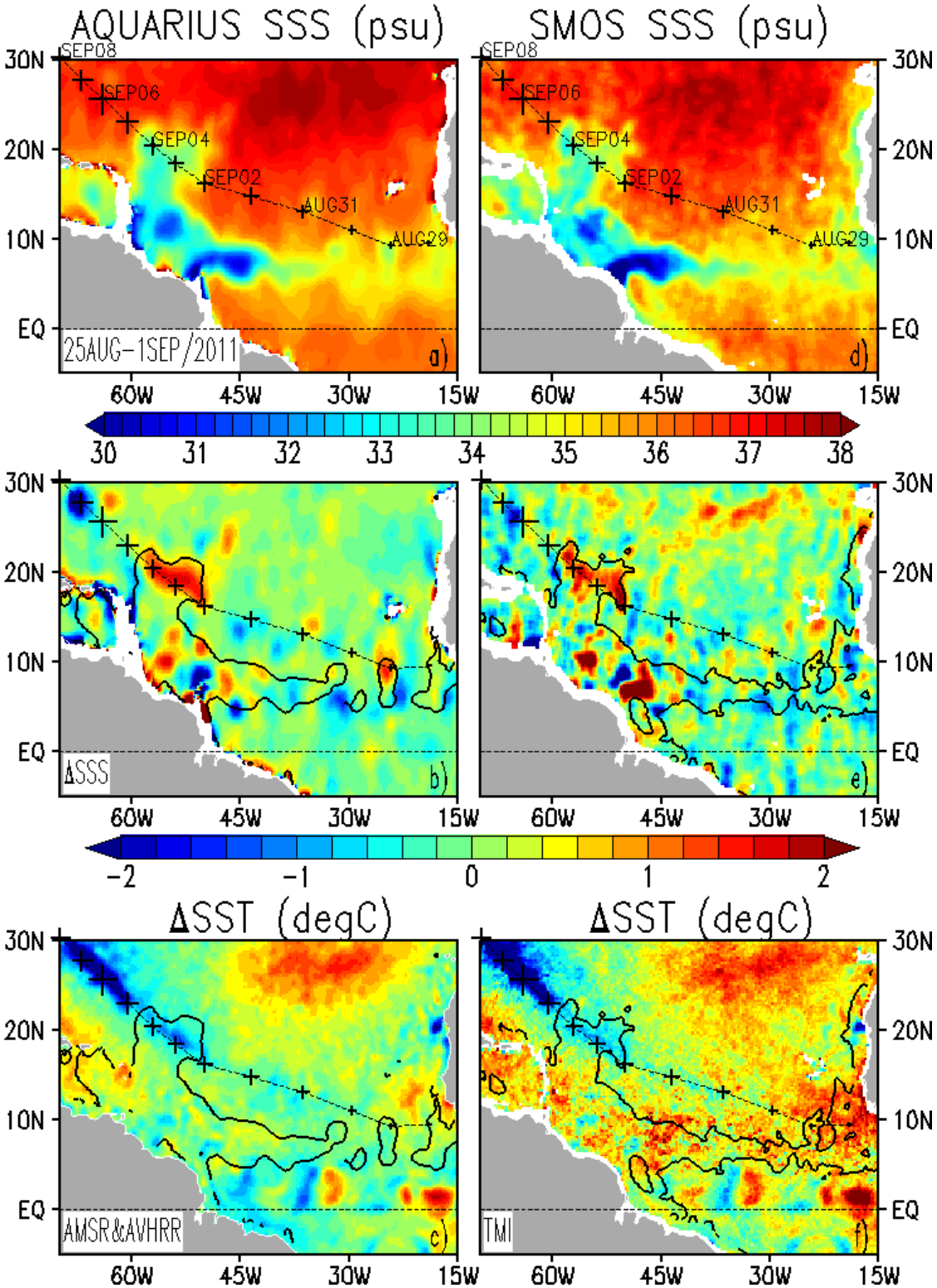

Figure 3. (left) AQUARIUS and (right) SMOS SSS (a,d) before hurricane Katia. Crosses are the hurricane daily position at 00:00UTC with size scaled between 20kt and 120kt of maximum sustained winds (from NHC analysis). (b,e) SSS and (c,f) SST differences after (5-10 SEP/2011) minus before (25AUG-1SEP/2011) the hurricane passage. 35 psu contour before the passage of Katia is overlain. The differences are color-scaled between -2 and 2. Land-contaminated coastal data are blanked.

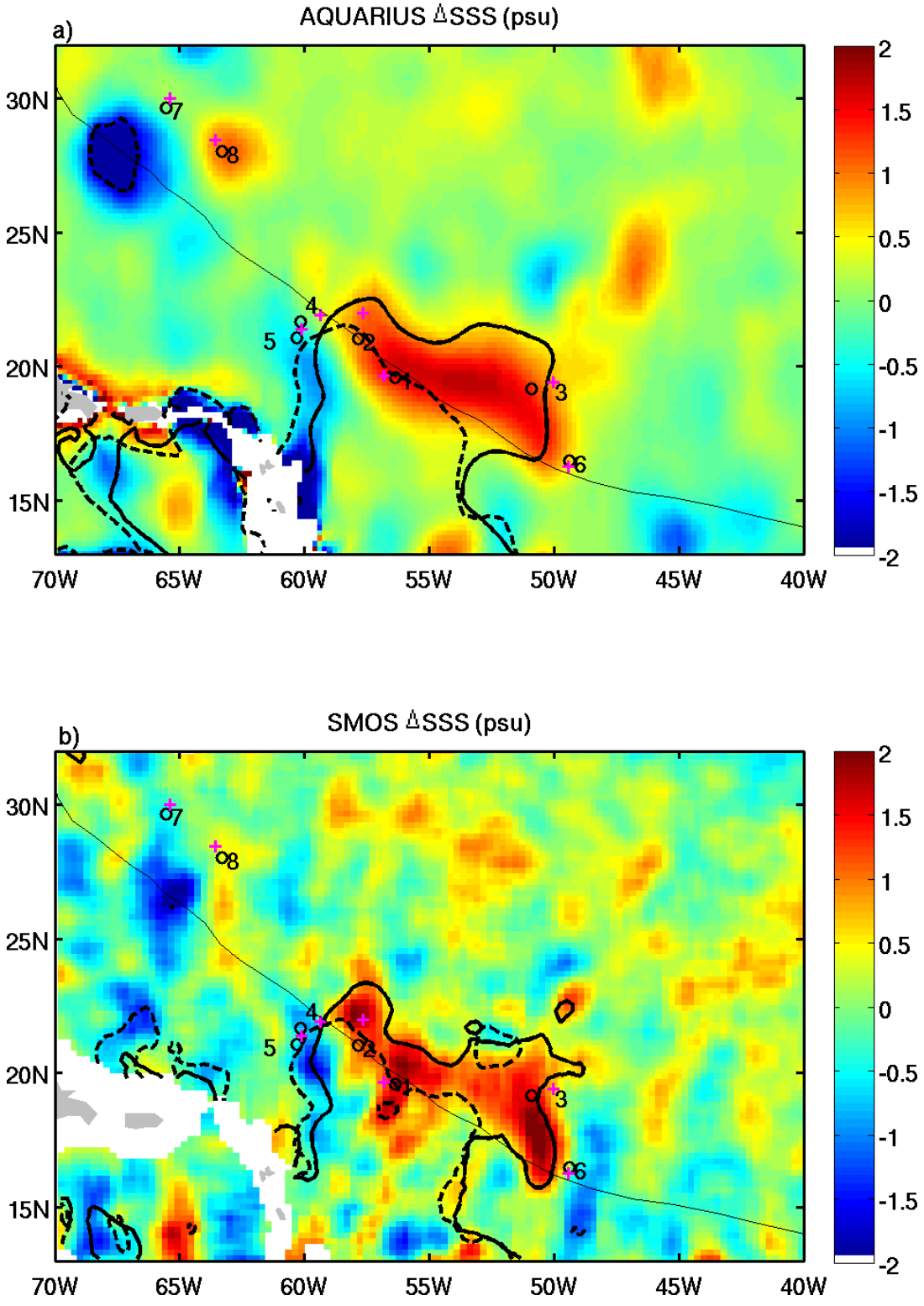

Figure 4. (a) Aquarius and (b) SMOS SSS difference (ΔSSS) between after (5-10 SEP/2011) minus before (25AUG-1SEP/2011) the passage of Katia. Location of Argo profiles before ('o') and after ('+') the passage. Bold solid and dashed are 35psu contour before and after the passage, respectively. Land-contaminated coastal data are blanked.

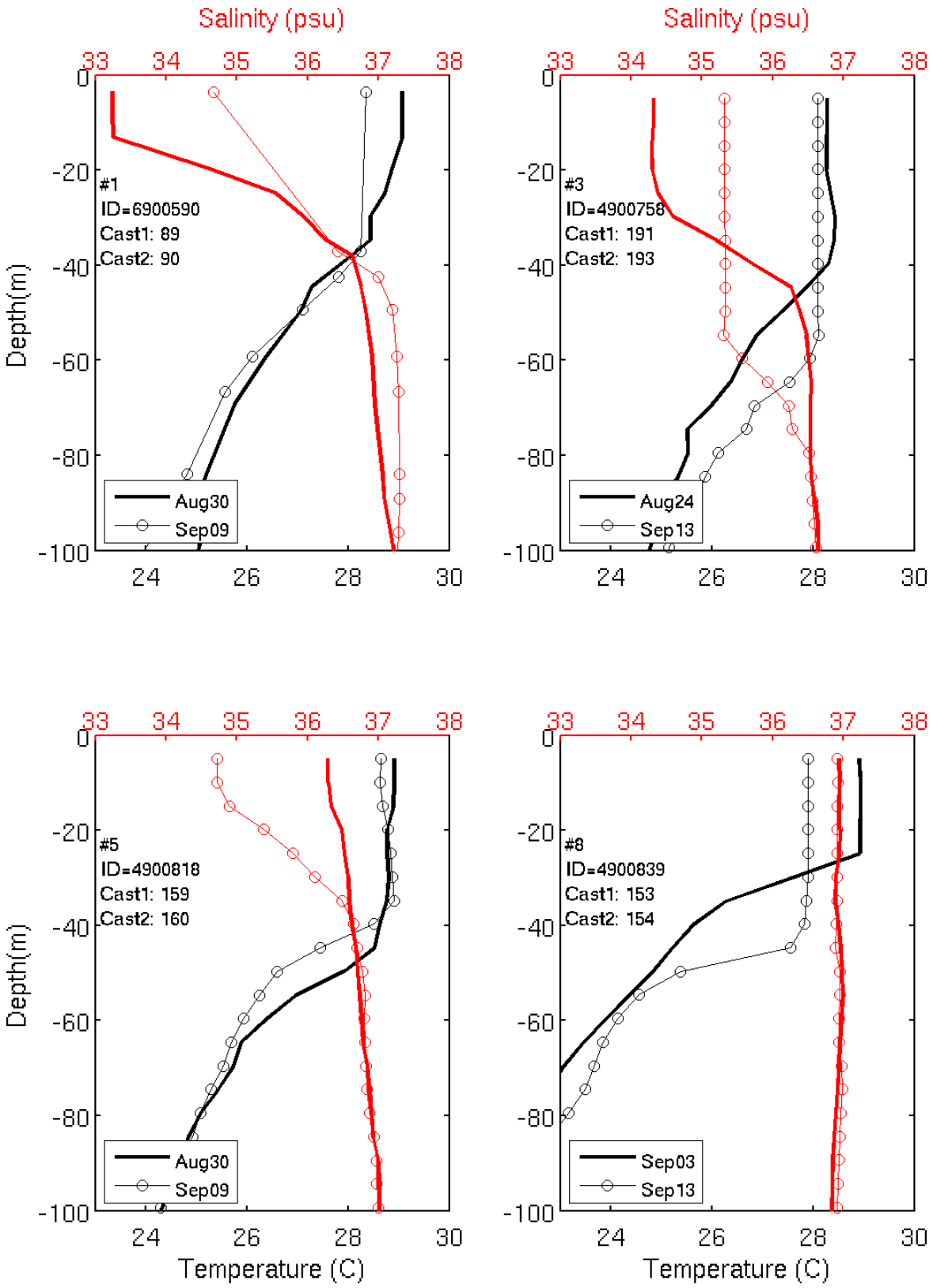

Figure 5. Argo profiles of temperature and salinity before (bold) and after (open circles) the passage of Katia (see Figure 4 for profile locations and Supplements for the rest of profiles).

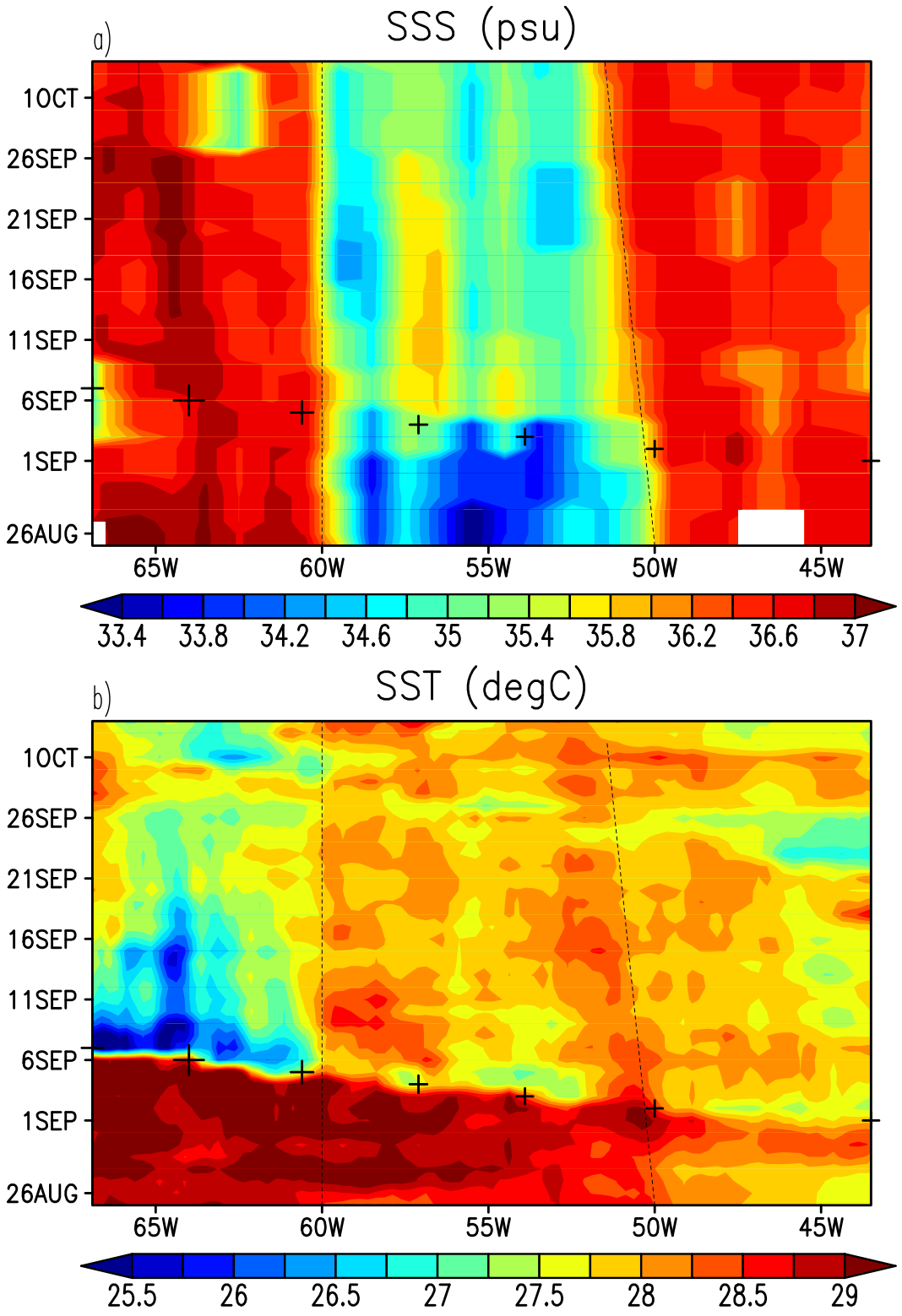

Figure 6. Temporal diagram of (a) weekly running mean AQUARIUS SSS and (b) SST along the hurricane track (see Fig. 5). Hurricane positions are overlain (see Fig.3 for marker scale). Fresh pool is encompassed by dashed lines. X-axis presents longitude along the track.

Supplementary Materials

Comparisons to the mooring salinity use same-day Aquarius salinity data (SSS_{AQ}) averaged over the four nearest grid points (corresponding to a roughly 200km spatial average) from the shallowest mooring level, which is 1 m depth in most cases. A preliminary comparison has allowed us to flag several mooring time series as unreliable, which have been removed from this comparison. More than 98% of the daily differences are less than 1psu, with a STD of daily data of 0.36 psu (Fig. S1). If we assume the errors are random the uncertainty would reduce to 0.25 psu for weekly means (approximately 10 Aquarius observations a month are available at each grid point). The mean bias is <0.1psu, but the histogram of differences shows significant fresh outliers. In fact systematic differences between *in situ* nearsurface salinity and satellite SSS may be expected in low salinity tropical regions where SSS is fresher than bulk salinity (Henocq et al., 2010). Reverdin et al. (2012) have found that individual rainfall-induced freshening events reduce salinities by an average 0.56 psu at 50 cm depth and amplify towards the surface, being larger by more than 20% at 15 cm below the surface. Our comparison (**Fig. S2)** of the much more limited set of spatially and temporally collocated Argo near surface salinity and Aquarius SSS in our region of interest during September to November, 2011 (when the plume is present) suggests a somewhat larger range of differences.

Both MW sensors indicate similar spatial patterns of haline changes in the wake of Katia (Fig. 4). Some differences between the two sensors are related to the differences in temporal coverage and spatial averaging, with the spatial smoothing being notorious for the Aquarius. Fig. S4 shows that due to better spatial resolution SMOS compares better with in-situ salinity changes (after minus before the passage of Katia) deducted from Argo profiles from Figs. 5 and S3 (see Fig. 4 for Argo locations).

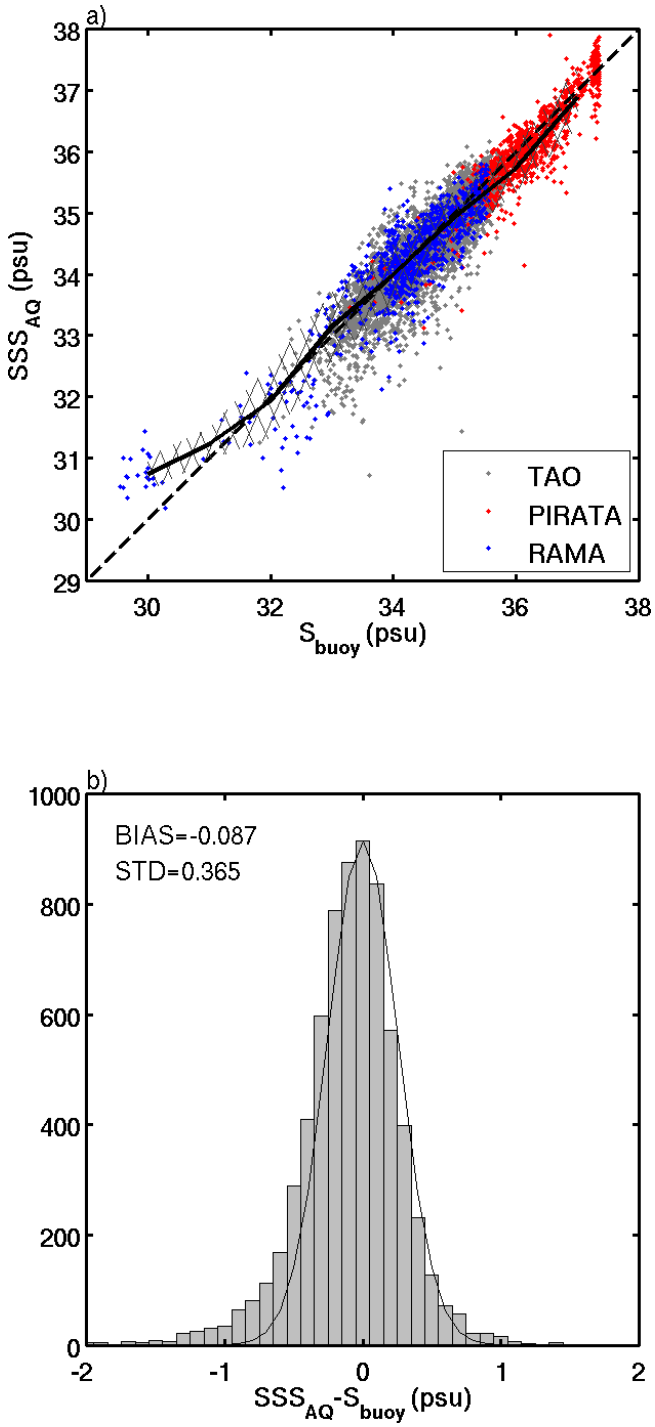

Figure S1 Comparison of daily mean 1m depth tropical mooring salinity (S_{buoy}) from the TAO/Triton, RAMA, and Pirata moorings (http://www.pmel.noaa.gov/tao/index.shtml) and contemporaneous, nearby AQUARIUS version 1.3 gridded SSS (SSS_{AQ}). (a) Scatter diagram of contemporaneous S_{buoy} and SSS_{AQ}. Solid line is mean SSS_{AQ} and cross-hatching shows ±σ as evaluated from S_{buoy} in 1 psu bins. (b) Histogram of differences divided into 0.1psu bins. Solid line is a least squares Gaussian fit. Bias and STD are shown in upper left.

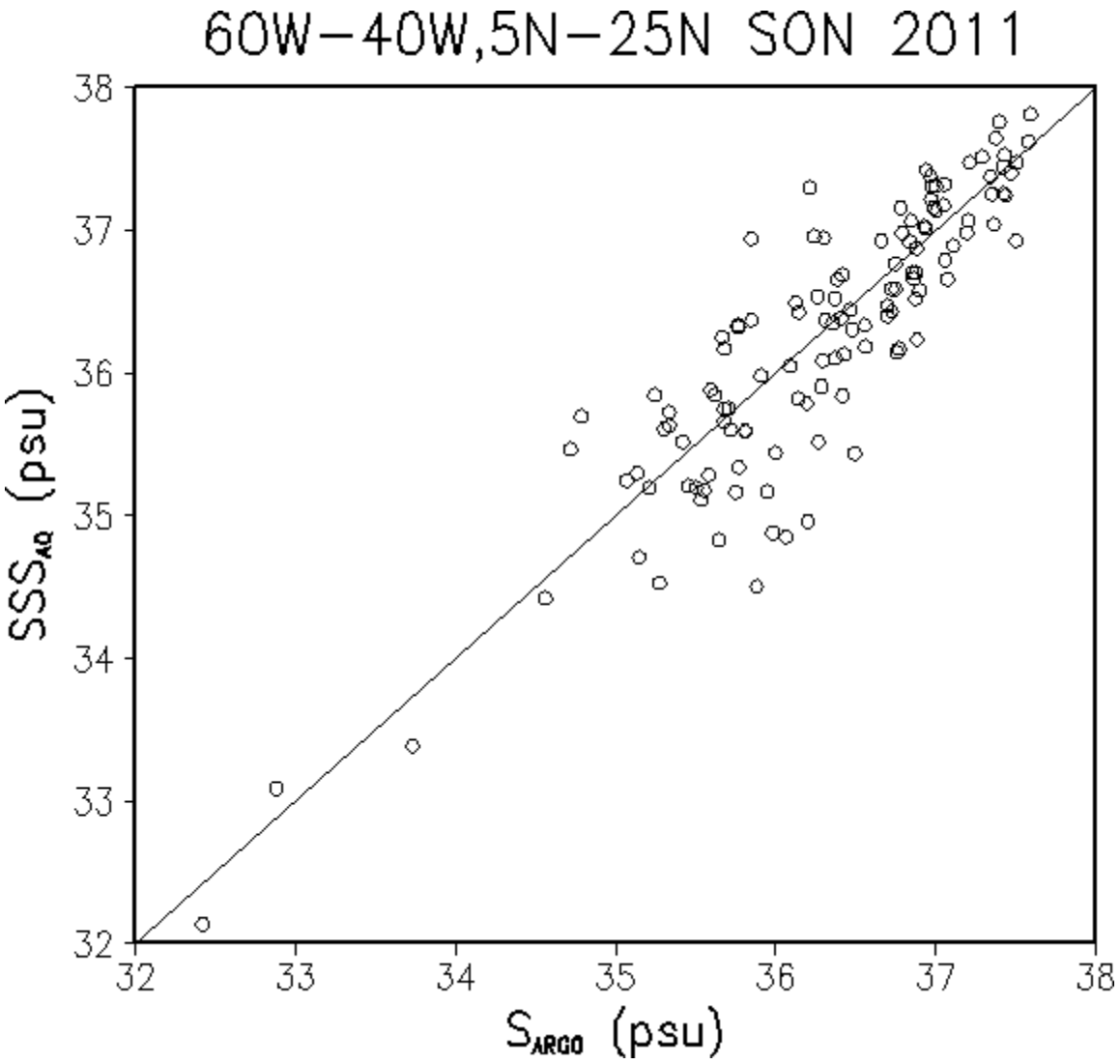

Figure S2. The same day AQUARIUS SSS and Argo float near surface salinity (the shallowest data from 5-10m depth range is taken, normally z=5m) in the western tropical Atlantic during the 2011 boreal fall.

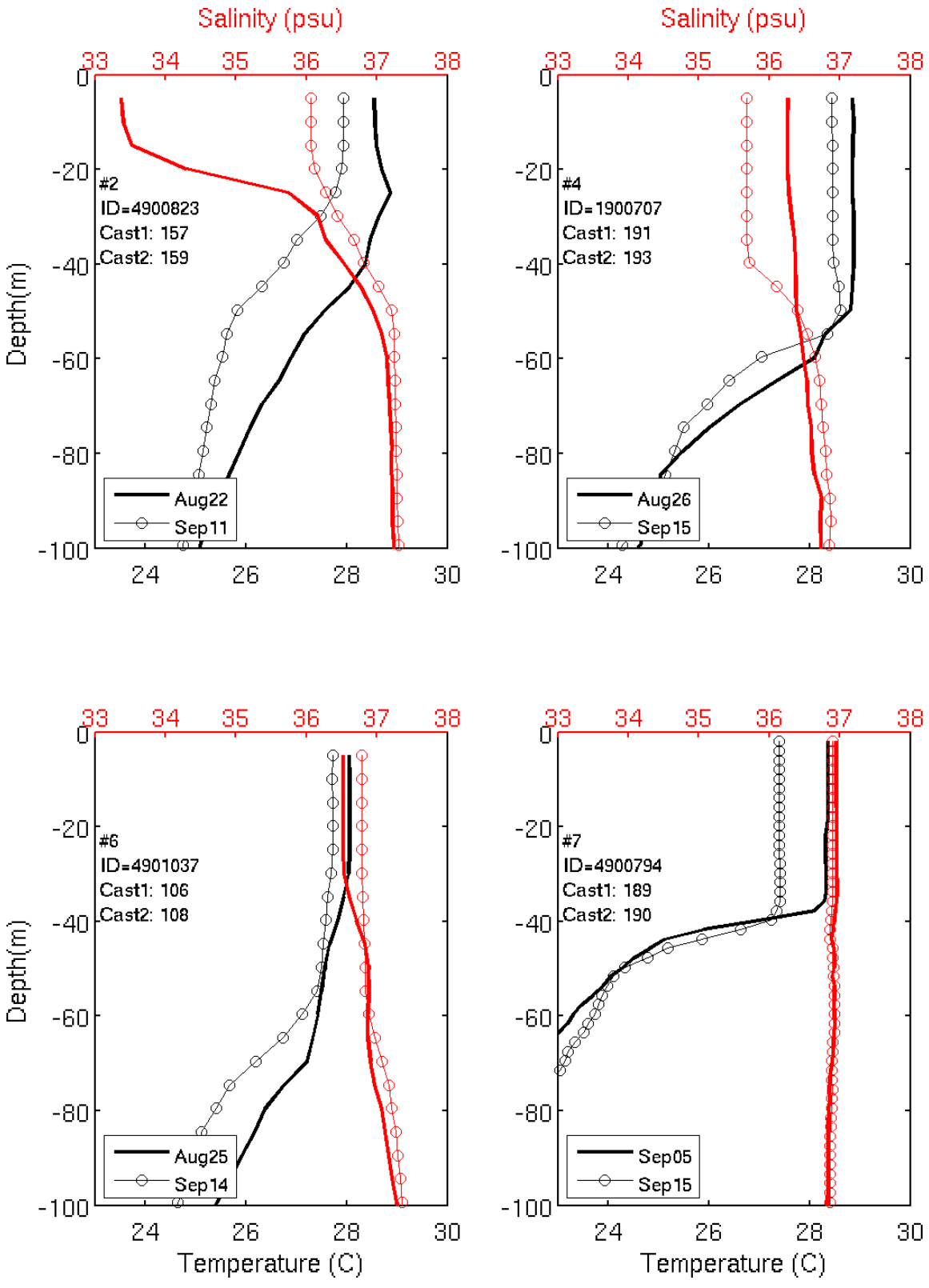

Figure S3. Vertical Argo profiles of temperature and salinity before (bold) and after (open circles) the passage of hurricane Katia (see Figure 4 for profile locations).

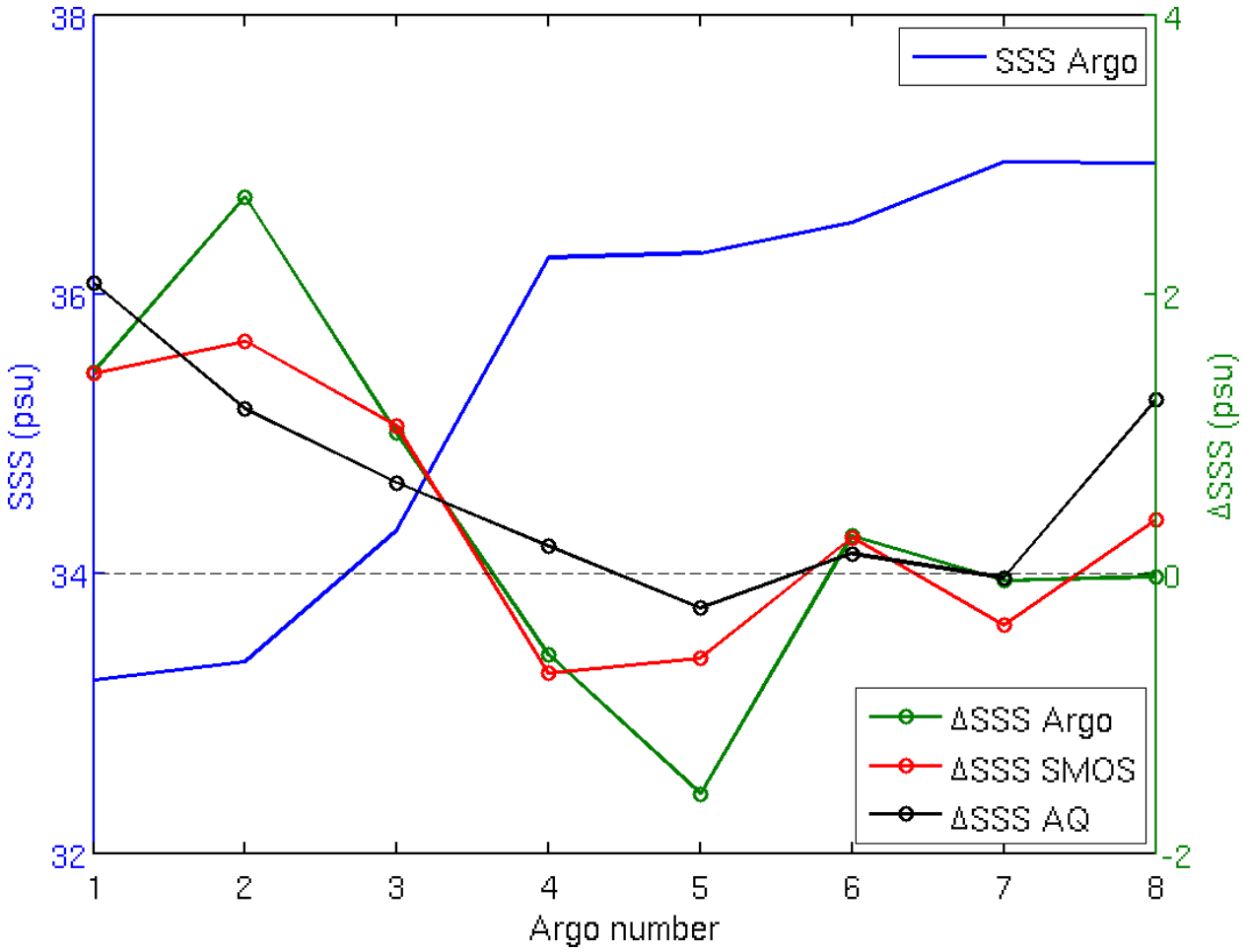

Figure S4. Near surface salinity change ΔSSS from Argo profiles and SMOS and Aquarius SSS change from Figures 4a, 4b. SSS before the passage of Katia is shown in blue.